

# Resolving the Turnover of Temperature Dependence of the Reaction Rate in Barrierless Isomerization

Jose-Luis Alvarez, Arkady Yartsev, Ulf Åberg, Eva Åkesson, and Villy Sundström\*

Department of Chemical Physics, Chemical Center, Lund University, Box 124, 221 00 Lund, Sweden

Received: February 6, 1997; In Final Form: March 11, 1998

In this work, the temperature dependence of the barrierless *cis*–*trans* isomerization reaction in the excited state of 1,1'-diethyl-4,4'-cyanine (1144-C) has been investigated. Transient absorption kinetics as well as transient absorption spectra were measured at different temperatures and viscosities, making it possible to obtain dynamic information regarding the isomerization process at constant viscosity. Our experimental results suggest a crossover of the reaction rate from a negative temperature dependence (decreasing relaxation rate with increasing temperature) at low viscosities to a positive temperature dependence at higher viscosities. This crossover of the relaxation rate was observed to occur at  $\sim 17$  cP; the range of viscosities studied was from  $\sim 2$  to  $\sim 30$  cP. We discuss the origin of this turnover behavior in terms of the BFO (Bagchi, Fleming, and Oxtoby) theory and show that the turnover can be explained by this model, as the competition between two processes following the excitation, namely transport of the population on the excited-state surface and internal conversion. We also discuss the validity of using the solvent shear viscosity as a measure of the friction experienced by the isomerizing group. Our results suggest that, at least for 1144-C in short-chain alcohols (methanol to hexanol), the shear viscosity can indeed be used as a reasonable measure of the solvent friction in the barrierless isomerization process.

## Introduction

In many isomerization reactions, the reaction coordinate is a large-amplitude motion of a bulky group twisting or rotating around a molecular axis. The target molecule of this study (shown in Figure 1) exhibits this type of reaction; the reaction coordinate involves a twisting motion around the C–C axis of one of the bonds of the methine bridge joining the two quinoline rings. These processes have been studied extensively as model reactions for testing theories of reaction dynamics in solution. The studies have focused mainly on reactions in which the large amplitude motion is associated with a high intramolecular potential energy barrier separating the reactant and product regions. The rate of such a reaction is mainly controlled by the height and shape of the barrier, but solute–solvent friction is also an important parameter;<sup>1–4</sup> most theoretical models used to explain experimental results of this type of reaction are related to the well-known theory of Kramers.<sup>5</sup> The potential barriers in these reactions are generally high compared with  $kT$ ; hence it is assumed that the isomerizing molecule is thermalized and vibrationally equilibrated during the process of concern. As a direct consequence of the high intramolecular barrier, these reactions show a strong positive, Arrhenius-type temperature dependence of the reaction rate.

Several chemical reactions, though, occur in the absence of any significant activation energy ( $E_a$ ) barrier. Examples include some *cis*–*trans* isomerizations,<sup>6–8</sup> excited-state dissociation reactions,<sup>9,10</sup> and some electron-transfer reactions<sup>11</sup> occurring in electronically excited states. From a biological perspective, the *cis*–*trans* isomerizations of rhodopsin<sup>12,13</sup> and bacteriorhodopsin,<sup>14–16</sup> the dissociation and recombination of dioxygen ( $O_2$ ) and carbon monoxide ( $CO$ )<sup>17</sup> in hemoglobin and myoglobin, and the primary electron transfer in the photosynthetic reaction center<sup>18</sup> can be mentioned as examples of zero-barrier

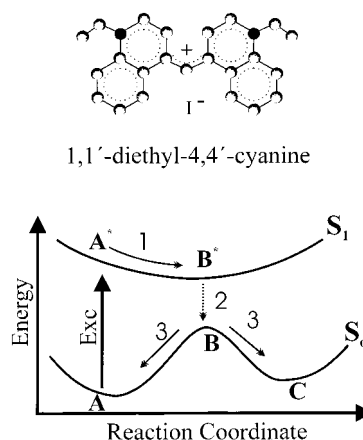


**Figure 1.** (a, top) 1,1'-Diethyl-4,4'-cyanine; (b, bottom) schematic of the one-dimensional potential energy surface representing the excited-state isomerization.

processes. Typical properties of the barrierless isomerization reactions are: high reaction rates, high quantum yield, and a temperature dependence of the reaction rate that is qualitatively different from that of the high barrier case. These reactions generally occur in an electronically excited state of the molecule; if the corresponding reaction occurs in the ground state, the potential barrier is normally much higher and the reaction is orders of magnitude slower. The time scale of the bond-twisting event on the excited-state surface is, for the barrierless case, of the same order of magnitude as intramolecular vibrational energy redistribution (IVR) and intermolecular cooling processes.<sup>19</sup> In addition, it is reasonable to assume that all of these processes compete with the  $S_1 \rightarrow S_0$  internal conversion. The relaxation of such a highly nonequilibrated system offers some particular problems that must be considered in the interpretation of different spectroscopic results. We have addressed these topics

in previous work on the barrierless excited-state isomerization of the cyanine molecule 1,1'-diethyl-4,4'-cyanine (1144-C)<sup>20–24</sup> (for structure see Figure 1). We have shown that the interplay between parameters such as the shape of the potential surface of the reaction coordinate, the location and shape of the relaxation funnel, the temperature, and the relevant friction between the solute and solvent molecules will all be critical for the rate and dynamics of the isomerization process.

Bagchi, Fleming, and Oxtoby (BFO)<sup>25</sup> provided a theoretical model of barrierless relaxation dynamics in the case of a large amplitude motion. In this model, the radiationless relaxation from the  $S_1$  to the  $S_0$  state is represented by a coordinate-dependent internal conversion funnel, the sink, centered at the position where the energy difference between the excited and ground-state potential surfaces is minimum. The radiative relaxation is represented by a position-independent sink distributed along the whole excited state potential surface. BFO further assume a one-dimensional harmonic potential surface that drives the molecules from reactant to product under the influence of solvent friction, and they describe the relaxation dynamics using a modified Smoluchowski equation. In the BFO model, processes such as IVR, intermolecular vibrational cooling (IVC), and solvent dynamics are not considered; therefore this model might present a slightly oversimplified description of the bond-twisting reaction. The extent to which IVR, IVC, and solvent relaxation influence the bond-twisting process of 1144-C is difficult to determine precisely, but has been extensively discussed in an earlier publication<sup>20</sup> where it was concluded that these processes are not primarily responsible for the observed dynamics of the barrierless isomerization. Alternative relaxation models have also been extensively discussed in previous publications.<sup>20,22–24</sup> Although some aspect of the observed relaxation behavior may be explained with an alternative model, all observations available today taken together are best accounted for by the barrierless isomerization model. Therefore, we do not further repeat the arguments here but refer to the earlier work.<sup>20,22–24</sup>

Using the energy curves of the molecule 1144-C displayed in Figure 1, the relaxation processes associated with the barrierless isomerization as they emerge from a BFO analysis can be described as follows. Excitation to the highly nonequibrated initial position ( $A \rightarrow A^*$ ) on the excited-state surface triggers the isomerization reaction, which is initially characterized by a very fast transport of the population (overdamped wave packet motion) along the  $S_1$  surface toward the sink ( $B^*$ ); this corresponds to a twisting of the quinoline rings relative to each other from approximately  $\theta = 40^\circ$  to  $\theta = 90^\circ$ . The value  $\theta = 40^\circ$  for the ground-state species was obtained from crystallographic investigations by Yoshioka and Nakatsu.<sup>26</sup> The sink constitutes a strong nonradiative coupling to the ground state and is located at the bottom of the excited-state surface. This nonradiative coupling is responsible for a slower, but still on the picosecond-to-tens of picoseconds time scale,  $S_1$  to  $S_0$  radiationless transition (process 2, Figure 1), after which the molecules return to either their original ground state conformation or to the photoisomer (process 3, Figure 1). The observed rate of the  $B^*$  to B relaxation process in a particular solvent is determined by the solvent viscosity (see Figure 4). The intrinsic internal conversion rate is much higher, probably on the subpicosecond time scale.<sup>23</sup>

To examine the various processes suggested by the potential energy surface diagram of Figure 1, time-resolved absorption and fluorescence methods have been used.<sup>8,20–24</sup> The transient absorption spectrum of the isomerizing molecules will have

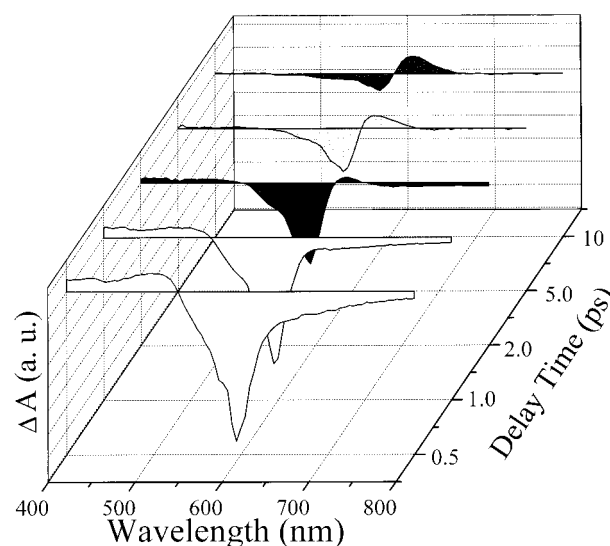


**Figure 2.** Measured transient absorption spectrum of 1144-C in hexanol at five different delay times. In the wavelength range 400–530 nm, a broad ESA is observed; in the range 550–630 nm a strong bleaching due to the ground-state depletion is observed. In the red part of the spectrum, ~630–800 nm, there is a broad SE band, and at later times also absorption at ~620 nm due to the ground-state photoisomer.

contributions from the bleaching of ground-state molecules, stimulated emission (SE), excited-state absorption (ESA), and additional absorption from ground-state photoisomers.<sup>22</sup> This implies that the transient absorption spectrum may be sensitive to all the processes indicated in Figure 1 and useful in monitoring the isomerization dynamics, both in the ground and excited states. Time-resolved fluorescence, however, is only sensitive to excited-state process and is therefore useful in distinguishing dynamics originating in ground and excited states. The barrierless dynamics measured with either method generally results in nonexponential kinetics with an early-time nonexponential part reflecting the initial bond-twisting (damped wave packet) process<sup>20,23</sup> and a slower exponential part reflecting the  $B^*$  to B internal conversion.<sup>22,23</sup> To examine the bond twisting process of 1144-C, both transient absorption<sup>22–24</sup> and time-resolved fluorescence<sup>20,24</sup> have been used. As an illustration to the results obtained, Figure 2 shows the temporal evolution of the transient absorption spectrum of 1144-C in hexanol, measured over the wavelength range 400–800 nm. In the wavelength range 550–630 nm a strong bleaching due to the ground-state depletion is observed. In the range ~630–800 nm there is a broad SE band, and at later times also absorption at ~620 nm due to the ground-state photoisomer. In the blue part of the spectrum, 400–530 nm, a broad ESA is observed. Kinetics and spectral changes of ESA and SE should give information about the dynamics in the excited-state reaction coordinate. The bond-twisting process is clearly manifested by wavelength-dependent SE kinetics;<sup>24</sup> in the red wing of the fluorescence band, the emission decay represents the overall excited-state lifetime, whereas the fluorescence at shorter wavelengths is strongly influenced by nonexponential transients originating from the transport of the population on the excited-state surface. This population transport on the excited-state surface should also be observable as a rise time of the spontaneous fluorescence kinetics measured in the red part of the fluorescence band. Previously, we resolved this in a fluorescence up-conversion experiment with a time-resolution of about 100 fs; the results show that bond-twisting occurs on a 300 fs to 1 ps time scale, and is dependent on solvent

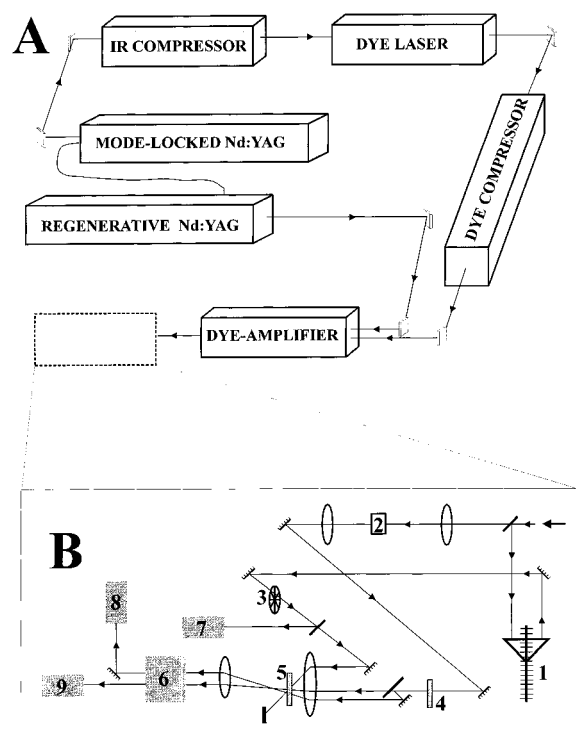


**Figure 3.** (A) Schematic arrangement of the amplified fs laser system; (B) Schematic experimental setup for pump-probe spectroscopy. 1, Delay line; 2, water continuum generation cell; 3, chopper; 4, dye DQOCI; 5, sample; 6, monochromator; 7, 8, and 9, photodiodes.

viscosity,<sup>23</sup> in good agreement with the conclusions of time-resolved SE and ESA experiments.<sup>23</sup>

As was discussed above, the BFO model (and extensions based upon it<sup>27–32</sup>) as well as similar models<sup>11,33</sup> have been used to predict the dynamics of barrierless isomerization reactions in the condensed phase. One of the most interesting predictions is a crossover of the temperature dependence of the long-time exponential decay rate. At low viscosities, the relaxation rate is predicted to decrease with increasing temperature, corresponding to an effective negative  $E_a$ ; on the other hand, at high viscosities, the behavior is predicted to be the opposite: the relaxation rate should increase with increasing temperature, implying a positive  $E_a$ . The origin of this behavior is a result of the interplay between the different viscosity-dependent processes constituting the barrierless reaction (see also *Discussion* and ref 25).

In the present work, we have studied the temperature dependence of the barrierless relaxation of 1144-C in alcohol solutions, and resolved the turnover from negative to positive temperature dependence of the relaxation rate as the viscosity is increased.

## Experimental Section

The transient absorption experiments in this work were performed with a spectrometer, based on amplified (1 kHz)  $\sim 200$  fs dye laser pulses. These pulses were generated by the laser system displayed schematically in Figure 3. The 1064 nm, 100 ps output pulses of the mode-locked cw Nd:YAG laser were split into two parts:  $\sim 10\%$  was used to seed the regenerative Nd:YAG amplifier and the remaining  $\sim 90\%$  was compressed down to  $\sim 5$  ps in a fiber-grating compressor. These pulses were then frequency doubled to 532 nm in a KTP crystal and used to pump a rhodamine 6G dye laser, which at 590 nm delivered an average output power of  $\sim 200$  mW with a pulse

duration of  $\sim 400$  fs. To further improve the time resolution, the  $\sim 400$  fs dye laser pulses were compressed in a fiber-prism compressor, delivering  $\sim 90$  fs pulses. After amplification in a two-stage dye amplifier longitudinally pumped by the regenerative Nd:YAG pulses, 20  $\mu$ J pulses with a duration of  $\sim 150$  fs and a repetition rate of 1 kHz were obtained. The amplified pulses were split into two approximately equal parts, one for excitation of the sample and the other for generation of a white-light continuum used as probe light. The continuum was created by focusing the laser beam into a flow cell of water. To make the spectral distribution of the continuum reasonably flat, the intensity at 590 nm (the wavelength of the pump light) was reduced after the continuum generation cell with a dye solution of DQOCI.

Reference and signal beams were obtained by dividing the continuum in two parts; the two beams were then identically focused into the sample, but in different spots of the sample. Therefore only the signal beam was spatially overlapped with the excitation beam. Reference and signal beams were then focused onto the slit of a single-grating monochromator, which allowed selection of the analyzing wavelength. After the monochromator, both the signal and reference beams were detected by photodiodes and the ratio  $I/I_{\text{ref}}$  was calculated for every pulse, with and without the excitation pulse incident on the sample. Finally, the absorbance change caused by the excitation pulse was obtained from the expression  $-\Delta A = \log(I/I_{\text{ref}})_{\text{ex}} - \log(I/I_{\text{ref}})_{\text{no ex}}$  and only results from excitation pulses falling within a preset intensity window were used. When measuring time-resolved transient spectra, the wavelength chirp of the continuum was compensated by changing the time delay between the pump and probe pulses according to a preset calibration curve. The response function and zero-time position were obtained by using two-photon absorption in diphenyl hexatriene, or from the derivative of the rising edge of the ground-state bleaching of some suitable dye molecule. The absorption kinetics were analyzed by using a nonlinear least-squares fitting procedure, including deconvolution with the measured cross-correlation function of the actual pulses. The sample of 1144-C was obtained from Eastman Kodak and its purity was checked by absorption spectra. All solvents (n-alcohols) used in the experiments were of spectroscopic grade, and viscosities at different temperatures were obtained from the literature. A liquid  $N_2$  cryostat (Oxford Instruments) was used to control the temperature of the solution in all experiments and the sample was kept in a cell of 1 mm pathlength.

## Results

To study the temperature dependence of the barrierless isomerization process, we measured transient absorption kinetics and difference absorption spectra of 1144-C in various alcohol solutions (the n-alcohol series methanol–hexanol) at different temperatures. In this series of experiments, the viscosity was kept constant by simultaneously changing solvent and temperature. Provided that shear viscosity is a reasonably good measure of microscopic friction, this isoviscosity approach implies that isomerization rates were measured at constant friction and the observed variation of the reaction rate is hence directly related to the temperature dependence of the barrierless process. The validity of the isoviscosity approach will be discussed below.

Transient absorption kinetics and spectra were measured over the probe wavelength range of 450–770 nm, in the temperature interval 183–297 K, and for a viscosity range of 2–30 cP. The excitation wavelength was 590 nm throughout the experiments,

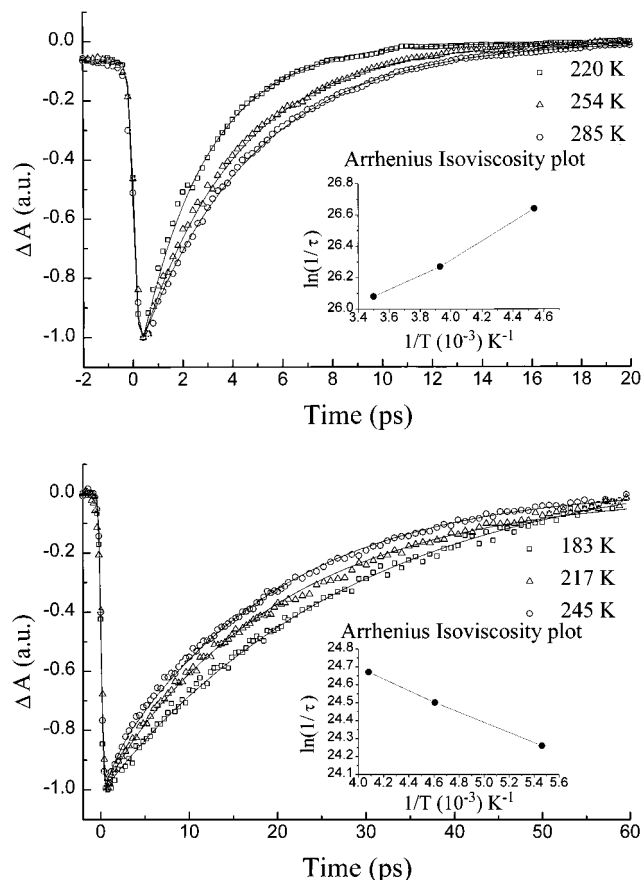


**Figure 4.** Measured decays and fits at 660 nm. (a, top) At 7 cP and three different temperatures:  $\square$ , 220 K in ethanol;  $\triangle$ , 254 K in propanol;  $\circ$ , 285 K in hexanol. Arrhenius isoviscosity plot is shown as inset. (b, bottom) At 30 cP and three different temperatures:  $\square$ , 183 K in ethanol;  $\triangle$ , 217 K in propanol;  $\circ$ , 245 K in hexanol. Arrhenius isoviscosity plot is shown as inset.

corresponding to the center of the ground-state absorption band. Figures 4a and 4b display the temporal evolution of the SE signal at 660 nm, at both low (7 cP) and high (30 cP) viscosities for three different temperatures. At a fixed viscosity of 7 cP, the decay measured at high temperature (285 K in hexanol) is observed to be slower than at lower temperatures (245 K in propanol and 220 K in ethanol); this corresponds to a negative temperature dependence as can be seen from the constant viscosity Arrhenius plot displayed in the inset of Figure 4a. At 30 cP (Figure 4b), the temperature dependence is reversed and the kinetics are faster at higher temperatures, indicating a positive temperature dependence (see inset). At an intermediate viscosity,  $\sim 17$  cP, the decays at all three temperatures are almost exactly superimposed, suggesting the absence of a significant temperature dependence at this viscosity. This behavior can also be observed in the ESA region, as is illustrated in Figure 5, where kinetics at 450 nm are presented for two different viscosities. Similar to the results in the SE region, the kinetics at 450 nm display a negative temperature dependence at 7 cP (Figure 5a) and a positive temperature dependence at higher viscosities, here illustrated by the kinetics measured at 27 cP (Figure 5b). From additional data at other viscosities (see Figure 8), we see that a crossover from a negative to a positive temperature dependence of the relaxation rate occurs, again at  $\sim 17$  cP. Thus, at low viscosities in the range 2–16 cP the relaxation rate decreases with increasing temperature, while in the viscosity range  $\sim 20$ –30 cP there is a “normal” (positive) temperature dependence of the relaxation rate. This behavior is not specific to a few discrete wavelengths, but rather can be

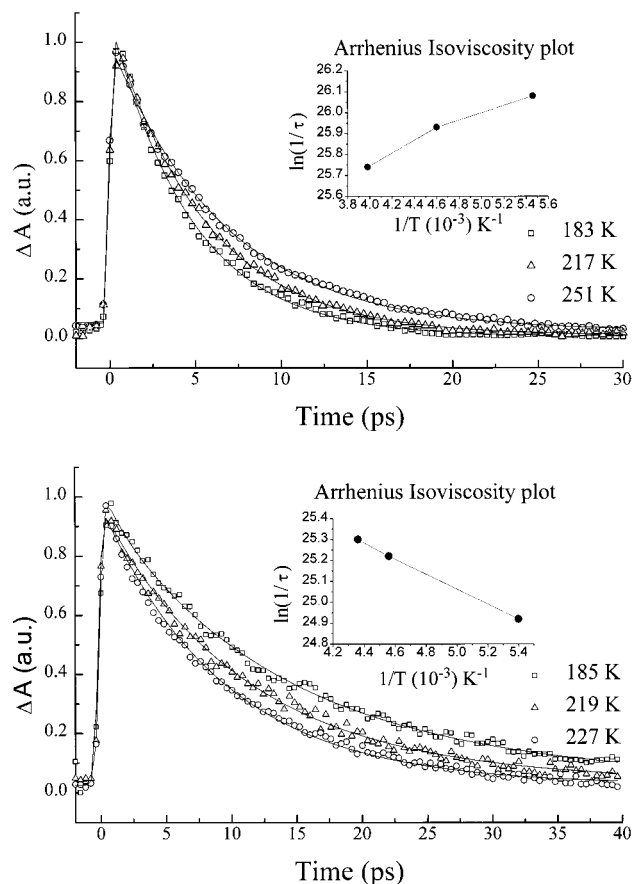


**Figure 5.** Measured decays and fits at 450 nm. (a, top) At 7 cP and three different temperatures:  $\square$ , 183 K in methanol;  $\triangle$ , 217 K in ethanol;  $\circ$ , 251 K in propanol. The corresponding Arrhenius isoviscosity plot is shown as inset. (b, bottom) At 27 cP and three different temperatures:  $\square$ , 185 K in ethanol;  $\triangle$ , 219 K in propanol;  $\circ$ , 227 K in butanol. The corresponding Arrhenius isoviscosity plot is shown as inset.

observed over the entire ESA and SE regions of the transient absorption spectrum, as demonstrated by the full transient absorption spectra in Figures 6 and 7, measured at two different temperatures and various delay times for two different viscosities. Each series of spectra measured at 7 and 22 cP demonstrates the different temperature dependencies of the excited-state relaxation dynamics of 1144-C at low (7 cP) and high (22 cP) viscosities. Figure 6 details the spectral evolution in the ESA (470–530 nm) and SE (620–680 nm) spectral regions for two different temperatures (220 K in ethanol and 287 K in hexanol) at 7 cP; solid lines represent the spectra measured at 220 K, whereas dotted lines represent the spectra at 287 K and different shapes represent the spectra at different times after excitation. In Figure 6 the lower temperature results in a faster decay of the ESA and SE signals. For instance, by comparing the two curves in Figure 6 with square symbols [filled squares on dashed curve (287 K) and open squares on solid line (220 K)] it is apparent that at 1 ps the ESA signal, at the lower temperature 220 K (Figure 6b), has had more decay (at zero delay time the two signals are normalized to the same intensity). A similar trend is seen at other times and also in the SE region (Figure 6c). This behavior is present until a substantial part of the signal has decayed after  $\sim 10$  ps. Figure 7 shows similar spectra to those of Figure 6, but at higher viscosity (22 cP). Solid lines represent the spectra measured at 189 K (in ethanol), whereas dotted lines represent the spectra at 256 K (in hexanol). At this viscosity, the temperature dependence of the rate of the studied process is weak and opposite to that at low viscosity.



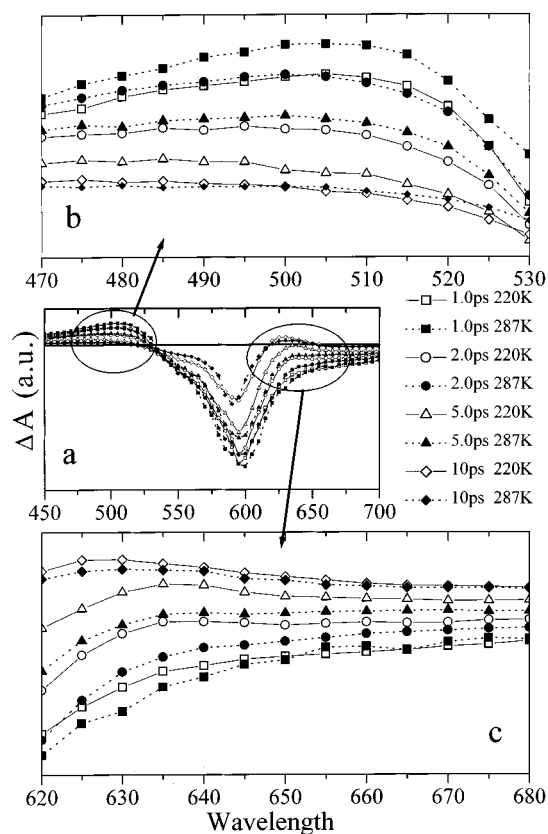


**Figure 6.** Transient absorption spectrum of 1144-C at 7 cP for four different delay times and two different temperatures, 220 and 287 K. Spectrum between (a) 450 and 700 nm; (b) 470 and 530 nm; (c) 620 and 680 nm.

In fact the viscosity chosen for Figure 7, 22 cP, is quite close to the turnover point at  $\sim 17$  cP, which explains the weak positive temperature dependence of the decay rate. At higher viscosities (e.g., 30 cP) the temperature dependence is stronger (see Figure 4b). It is important to notice that although the kinetics change by less than a factor of 2 over the temperature interval used at a given viscosity, the trend is significant and real; the observed changes exceed by several times the margin of error of our measurements and fitting procedures.

It should also be mentioned that to fit our kinetics, we used a nonlinear least-squares fitting procedure, including deconvolution with our instrument response function (the cross-correlation of the pump and probe pulses). As was mentioned earlier, kinetics monitoring the relaxation and decay of the 1144-C excited state are generally nonexponential, with a fast component reflecting the initial bond-twisting process (wave packet motion), followed by a slower exponential part associated with the decay of the equilibrated population from the sink. Since the present study is aimed at examining the temperature dependence of the slower exponential process, the probe wavelengths used to measure the kinetics, on which the isoviscosity plots are based (Figures 4, 5, and 8), were chosen to minimize the contribution of the fast process. When measuring SE kinetics this implies choosing a wavelength in the red wing of the fluorescence spectrum, which essentially monitors the integrated decay of the excited-state population;<sup>23</sup> hence the use of 660 and 770 nm in Figures 4 and 8. For ESA kinetics the same situation can be accomplished by choosing a probe wavelength in the center of the ESA band<sup>23</sup> (Figure 5). As a result of this wavelength choice we could fit all kinetic data to monoexponential functions, and small deviation from these fits in the very early part at the kinetics did not

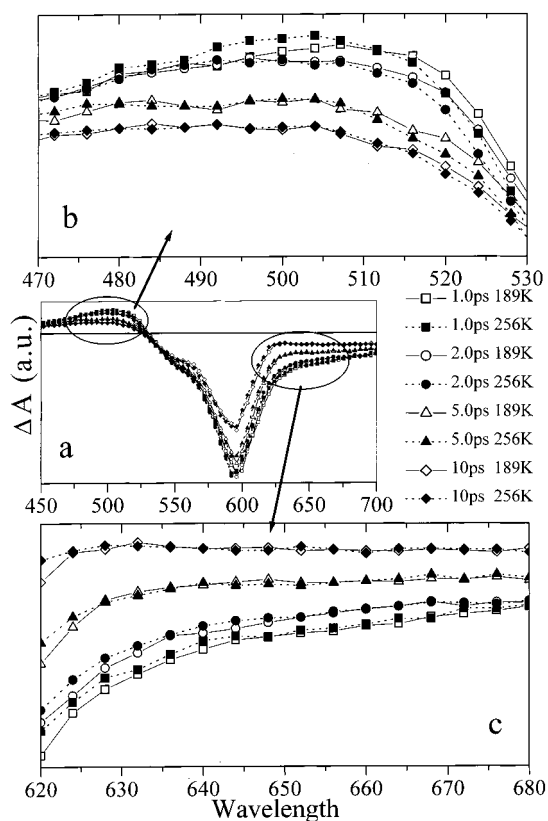


**Figure 7.** Transient absorption spectrum of 1144-C at 22 cP for four different delay times and two different temperatures, 189 and 256 K. Spectrum between (a) 450 and 700 nm; (b) 470 and 530 nm; (c) 620 and 680 nm.

substantially influence the obtained lifetimes. The lifetimes obtained from fits to the kinetic data in Figures 4 and 5 are summarized in Table 1.

Although a barrierless reaction lacks a real  $E_a$ , one can construct isoviscosity Arrhenius plots based on the kinetics measured at one viscosity and several temperatures to deduce information about the response of the reaction to a change of temperature. In this case, the slope of the plot is only an apparent  $E_a$ , not an actual activation barrier height. A few examples of such isoviscosity plots are presented as insets of Figures 4 and 5. In Figure 8, a more complete set of constant viscosity Arrhenius plots are shown for three wavelengths (450, 660, and 770 nm) and three different viscosities. As previously indicated by the temperature dependence of the kinetics measured at various wavelengths (Figures 4 and 5), the isoviscosity plots constructed for the three different wavelengths all show a similar variation with viscosity. At low viscosity ( $< 16$  cP) the lines fitted to the data points have a positive slope, which indicates an apparent negative  $E_a$  of the reaction. For intermediate viscosities ( $\sim 16$ – $20$  cP), the slope is very close to zero, while at high viscosities ( $> 20$  cP), the plots have a negative slope, suggesting an apparent positive  $E_a$ . These plots are useful for visualizing the temperature effect and for quantitatively determining the viscosity corresponding to the turnover point from negative to positive  $E_a$ . Both the isoviscosity plots and transient absorption spectra directly show that the turnover of the temperature dependence of the reaction rate in 1144-C occurs at 16–20 cP.

An alternative method to obtain information about the magnitude of the intrinsic activation barrier,  $E_a$ , is the so-called medium enhanced barrier model introduced by Saltiel and co-workers.<sup>34,35</sup> The model states that the total activation energy,

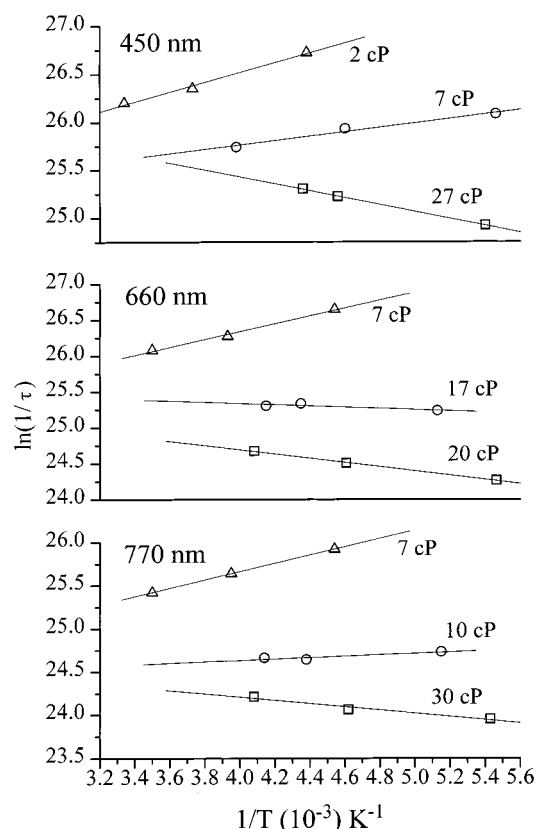


**Figure 8.** Arrhenius isoviscosity plots and fits at 450, 660, and 770 nm.

**TABLE 1: Long-Time Exponential Relaxation Times of 1144-C at Various Viscosities in the Solvents Methanol to Hexanol<sup>a</sup>**

wavelength (nm)	viscosity (cP)	solvent	lifetime (ps)
450	~2	methanol	2.48
		ethanol	3.60
		propanol	4.17
	~7	methanol	4.68
		ethanol	5.46
		propanol	6.62
	~27	ethanol	15.03
		propanol	11.10
		butanol	10.23
660	~7	ethanol	2.69
		propanol	3.89
		hexanol	4.69
	~17	ethanol	10.94
		propanol	9.97
		butanol	10.28
	~30	ethanol	28.86
		propanol	22.71
		hexanol	19.13

<sup>a</sup> The lifetimes are obtained from exponential fits to the data in Figures 4 and 5. These lifetimes are used to construct the isoviscosity plots of Figure 4, 5, and 8.

$E_{\text{tot}}$ , has contributions from  $E_a$  and the solvent viscosity activation energy,  $E_\eta$ , according to the relation  $E_{\text{tot}} = E_a + aE_\eta$  ( $0 \leq a \leq 1$ ). By measuring  $E_{\text{tot}}$  of a reaction in solvents of different  $E_\eta$  and extrapolating to  $E_\eta = 0$ ,  $E_a$  may be estimated. When this was done for *cis*-stilbene<sup>36</sup> in alkanes, a negative value of  $E_a$  was obtained, indicating a barrierless isomerization. However, for a barrierless process exhibiting BFO dynamics we do not expect  $E_a$  to be constant (independent of temperature and viscosity), as strongly suggested by our results for 1144-C. In this case the medium enhanced model would not be applicable. The isomerization rate of *cis*-stilbene has been

shown to have a viscosity dependence qualitatively different from that expected for a barrierless process of the BFO type. To explain this viscosity dependence of *cis*-stilbene isomerization a potential surface including a low potential barrier was suggested,<sup>37</sup> rather than the shallow barrierless surface observed for a typical BFO process.

## Discussion

Having shown that the long-time exponential part of the barrierless relaxation rate has a turnover from apparent negative  $E_a$  at low viscosities to an apparent positive  $E_a$  at higher viscosities (with a turnover point at ~17 cP), we will now discuss this result in relation to the prediction of the BFO theory<sup>25</sup> of negative  $E_a$  and turnover to positive  $E_a$ .

Several previous studies of barrierless isomerization have demonstrated an apparent negative  $E_a$  at some viscosities and in some solvents, but the negative temperature dependence was generally considered to have an origin other than the BFO negative  $E_a$ . For instance, a negative  $E_a$  was observed by Ben-Amotz and Harris for crystal violet<sup>38</sup> and concluded to be a result of a temperature-induced change of the ground-state torsional distribution of the phenyl rings. Such a change would shift the initial position of the excited-state population so as to give rise to a decrease in the reaction rate with increasing temperature. A turnover from negative to positive temperature dependence of the relaxation rate of crystal violet and ethyl violet in long-chain alcohols was also observed<sup>8</sup> and attributed to a solvent-induced change of the potential energy surface. Similarly, previous observations of the negative temperature dependence of the isomerization rate of 1144-C in alcohols were tentatively attributed to similar effects, i.e., temperature-induced changes of the potential energy surface or to a shift along the reaction coordinate of the excited-state potential surface with respect to the ground-state potential.<sup>8</sup>

In contrast, our Monte Carlo simulations based on the Smoluchowski equation (modified for the barrierless case<sup>25</sup>) suggested the presence of an intrinsic negative temperature dependence of the long-time relaxation rate.<sup>23</sup> A comparison of these theoretical results and the present experimental results of the temperature dependence of the 1144-C isomerization rate shows that the theoretically predicted negative temperature dependence of the long-time exponential rate occurs at similar viscosities and is of the same order of magnitude as that observed experimentally. This agreement supports the idea that the BFO model describes, at least qualitatively, the temperature dependence of the relaxation rate of barrierless isomerization reactions in solution.

To better understand whether the observed temperature dependence of the isomerization rate of 1144-C, and in particular the turnover from apparently negative to positive  $E_a$ , is of the intrinsic origin predicted by the BFO model, it is useful to examine the underlying physical process behind this behavior. The nature of the turnover can be explained as follows: After preparing the population on the excited-state surface, the overall process, which takes the molecule from the initially excited state to the ground state, involves a bond-twisting event followed by  $S_1 \rightarrow S_0$  radiationless relaxation. At low viscosities, this bond-twisting occurs on a subpicosecond time scale and becomes slower at higher viscosities.<sup>20,23</sup> The rate of relaxation (via the sink) to the  $S_0$  ground state depends on the instantaneous, but thermally determined, concentration of molecules (density of population) directly over the sink. Therefore the population of the ground vibrational level in the excited state is crucial for the relaxation rate. At low viscosities, when the transport to

the sink is subpicosecond and the dynamics within the population are fast, the quasi-equilibrium density over the sink will determine the  $S_1 \rightarrow S_0$  relaxation rate. Lowering the temperature from some particular value implies a narrowing of the population distribution and an increase of the population density over the sink; hence the relaxation rate increases with decreasing temperature.<sup>23</sup> This behavior corresponds to an apparent negative  $E_a$ . The assumption of a quasi-equilibrium density over the sink after the transport on the excited-state surface and possible other explanations to this fast relaxation have been discussed in detail in an earlier publication;<sup>20</sup> briefly, the time scale of the initial relaxation assigned to the transport process seems to be too slow to be explained with IVR processes and too fast to be attributed to the IVC and solvation processes in these types of solvents. As the viscosity is increased, at some point the rate of transport of the excited-state population along the reaction coordinate becomes comparable with the  $S_1 \rightarrow S_0$  relaxation rate and the dynamics within the equilibrated population slows down. At these viscosities, an increase of temperature (and corresponding increase of kinetic energy along the reaction coordinate) leads to a higher overall relaxation rate and consequently an apparent positive  $E_a$ . An estimate of the viscosities at which this behavior will occur is provided by measurements of the delayed onset of ground-state recovery<sup>23</sup> or the rise time of long wavelength fluorescence originating from the sink region.<sup>20</sup> These experiments indicate that at viscosities in the range  $\sim 2$ – $5$  cP, the bond twisting process occurs on the  $\sim 1$ – $3$  ps time scale. At  $\sim 17$  cP, where the turnover of the temperature dependence occurs, the excited-state bond-twisting process is expected to proceed on the  $\sim 5$ – $10$  ps time scale, which is quite comparable with the  $S_1 \rightarrow S_0$  relaxation rate. As is illustrated by the time-resolved spectra of Figure 2, the ground-state photoisomer absorbs maximally at  $\sim 625$  nm. The appearance of the photoisomer at times  $5$ – $10$  ps after excitation also at the highest viscosities (22 cP, Figure 7), evidenced by a dip at 625 nm in the broad SE band, is further evidence that bond-twisting occurs on the  $5$ – $10$  ps time scale at the viscosities of turnover.

The use of isoviscosity plots to obtain the temperature dependence of the barrierless isomerization rate relies on the assumption that the shear viscosity is a reasonably good measure of the microscopic friction experienced by the isomerizing group. We now turn to a brief discussion of the validity of this assumption. A proper description of friction is one of the most important tasks in condensed-phase reaction dynamics and much effort has been devoted to the problem.<sup>39</sup> As an example, we can consider the Kramers model,<sup>5</sup> in which the reaction rate is expressed as a function of properties of the potential energy surface of the reaction coordinate as well as the friction exerted by the surrounding medium on the reacting molecule. This friction is a measure of the collision frequency and type of interactions between the solvent and the reacting molecules.

An often-used description of friction is the molecule-nonspecific, hydrodynamic description, in which the friction recognized by the isomerizing group of the molecule is assumed to be proportional to the shear viscosity of the solvent.<sup>5</sup> This approach is based on the Brownian motion description, in which the molecular nature of the solvent is neglected since it is assumed that the isomerizing group is much larger than the solvent molecules. The hydrodynamic description of friction appears to work quite well for reactions with moderate barrier and as long as similar solvents are considered, e.g., a series of alkanes or *n*-alcohols,<sup>4,39–43</sup> yet there are also many examples in the literature where macroscopic shear viscosity fails to

describe the microscopic friction.<sup>1–3,37,44–46</sup> Special attention has been devoted to studies of the friction–viscosity relation for isomerization reactions with a considerable potential barrier. A large body of evidence shows that the Stoke–Einstein relation often breaks down for high-viscosity solvents, fast reaction rates (i.e., rate of barrier passage), or high intramolecular barriers.<sup>1–3,34,35,37,44–47</sup> On the other hand, other studies indicate that for reactions with a low<sup>39–43</sup> or zero<sup>48,49</sup> potential barrier and consequently relatively slow motion in the transition state region, the Stoke–Einstein relation applies.

To improve the hydrodynamic description, many approaches have been explored that attempt to account for various aspects of microscopic friction. Frequency-dependent friction has been found to be important in barrier crossing reactions having a sharp barrier,<sup>48,50,51</sup> and the contribution of free volume effects to friction has also been manifested for rotational reorientation as well as isomerization<sup>4,25,52,53</sup> processes. An empirical approach to a microscopic description of friction in isomerization reactions, used with some success,<sup>54–56</sup> is to use the rotational correlation time of a molecule similar to the reaction fragment as a measure of the friction during the reaction.

In the case of the barrierless reaction presented here, frequency-dependent friction is expected to be less important (due to the lack of a potential barrier and therefore slow motion through the transition-state region), but excluded volume effects could contribute significantly to the microscopic friction. To find out to which extent such effects may influence our results, we have examined the relation between rotational reorientation times and shear viscosity for the dye molecule 3,3'-diethyloxadicyanocyanine iodide (DODCI) in alcohols (methanol–hexanol, octanol, decanol), as provided by the measurements in ref 39. The 1144-C and DODCI molecules are both cyanine dye molecules of about the same size and shape. We therefore expect that the rotational reorientation times of DODCI in alcohols will provide a good measure of the microscopic friction sensed by 1144-C, in the course of barrierless isomerization, in the same solvents (the fact that 1144-C isomerizes quickly makes it very difficult to accurately measure the rotational relaxation time for this molecule). When plotting the rotational reorientation times ( $\tau_{or}$ ) of DODCI in alcohols<sup>39</sup> as a function of shear viscosity, the first four normal alcohols fall on a straight line, whereas hexanol is somewhat off this line. The slope of this line also closely corresponds to the estimated hydrodynamic volume of the DODCI molecule. This implies that for the solvents used in our work (methanol–butanol and hexanol), there is only a small deviation (solvent hexanol) from the linear Stokes–Einstein relation between rotational relaxation time (microscopic friction) and shear viscosity. It is therefore highly unlikely that a changed viscosity–microfriction relation through the solvent series will distort the observed dependence on viscosity of the barrierless  $E_a$ . This possibility becomes even more unlikely when it is noted that the same solvents, or at the maximum one different, were used in both the low- and high-viscosity isoviscosity Arrhenius plots.

## Summary

In the present work, we have studied the temperature dependence of the barrierless isomerization reaction of 1144-C. To obtain dynamic information regarding the isomerization process, we measured transient absorption kinetics as well as transient absorption spectra at different temperatures and viscosities.

Our experimental results resolve the crossover of the reaction rate from a negative temperature dependence at low viscosities

to a positive temperature dependence at higher viscosities. This crossover of the relaxation rate occurs at  $\sim 17$  cP. Specifically, at low viscosities in the range of  $\sim 2$ – $16$  cP, the relaxation rate decreases with increasing temperature, whereas for higher viscosities, there is a normal positive temperature dependence of the rate. These results are in agreement with predictions of the BFO theory that the temperature dependence of the decay in the barrierless isomerization is controlled by the competition between motion to the sink and removal of population from the sink region. From our considerations of the friction-viscosity relation we can conclude that, at least for 1144-C in small-molecule alcohols, shear viscosity can be used as a measure of the solvent friction in the barrierless isomerization process.

**Acknowledgment.** We gratefully acknowledge financial support from the Swedish Natural Science Research Council and the Knut and Alice Wallenberg foundation.

## References and Notes

- (1) Courtney, S. H.; Fleming, G. R. *J. Chem. Phys.* **1985**, *83*, 215.
- (2) Sun, Y. P.; Saltiel, J. J. *J. Phys. Chem.* **1989**, *93*, 8310.
- (3) Doany, F. E.; Heilweil, E. J.; Moore, R.; Hochstrasser, R. M. *J. Chem. Phys.* **1984**, *80*, 201.
- (4) Åkesson, E.; Hakkarainen, A.; Laitinen, E.; Helenius, V.; Gillbro, T.; Korppi-Tommola, J.; Sundström, V. *J. Chem. Phys.* **1991**, *95*, 6508.
- (5) Kramers, H. A. *Physica*. **1940**, *4*, 284.
- (6) Oster, G.; Nishijima, Y. *J. Am. Chem. Soc.* **1956**, *78*, 1581.
- (7) Sundström, V.; Gillbro, T.; Bergström, H. *Chem. Phys.* **1985**, *73*, 439.
- (8) Åkesson, E.; Bergström, H.; Sundström, V.; Gillbro, T. *Chem. Phys. Lett.* **1986**, *126*, 385.
- (9) Harris, A. L.; Berg, M.; Harris, C. B. *J. Chem. Phys.* **1986**, *84*, 788.
- (10) Harris, A. L.; Brown, J. K.; Harris, C. B. *Annu. Rev. Phys. Chem.* **1988**, *39*, 341.
- (11) Sumi, H.; Marcus, R. A. *J. Chem. Phys.* **1986**, *84*, 4894.
- (12) Buchert, J.; Stefancic, V.; Doukas, A. G.; Alfano, R. R.; Callender, R. H.; Akita, H.; Balogh-Nair, V.; Sakanishi, K.; Pande, J. *Biophys. J.* **1983**, *43*, 279.
- (13) Doukas, A. G.; Junnagar, M. R.; Alfano, R. R.; Callender, R. H.; Kokitani, T.; Honig, B. *Proc. Natl. Acad. Sci. U.S.A.* **1984**, *81*, 4970.
- (14) Gillbro, T.; Sundström, V. *Photochem Photobiol.* **1983**, *37*, 445.
- (15) Mathies, R. A.; Cruz, C. H. B.; Pollard, W. T.; Shank, C. V. *Science*, **1988**, *240*, 777.
- (16) Pollard, W. T.; Cruz, C. H. B.; Shank, C. V.; Mathies, R. A. *J. Chem. Phys.* **1989**, *90*, 199.
- (17) Cantor, C. R.; Schimmel, P. R. In *Biophysical Chemistry: The Behavior of Biological Macromolecules*; Bartlett, A. C., Vapnek, P. C., McCombs, L. W., Eds.; W. H. Freeman and Co.: New York, 1980.
- (18) Van Grondelle, R.; Dekker, J.; Gillbro, T.; Sundström, V. *Biochim. Biophys. Acta*, **1994**, *1187*, 1.
- (19) Elsaesser, T.; Kaiser, W. *Annu. Rev. Phys. Chem.* **1991**, *42*, 83.
- (20) Yartsev, A.; Alvarez, J. L.; Åberg, U.; Sundström, V. *Chem. Phys. Lett.* **1995**, *243*, 281.
- (21) Bagchi, B.; Åberg, U.; Sundström, V. *Chem. Phys. Lett.* **1989**, *162*, 227.
- (22) Åberg, U.; Åkesson, E.; Fedchenia I.; Sundström, V. *Isr. J. Chem.* **1993**, *33*, 167.
- (23) Åberg, U.; Åkesson, E.; Alvarez, J. L.; Fedchenia, I.; Sundström, V. *Chem. Phys.* **1994**, *183*, 269.
- (24) Åberg, U.; Åkesson, E.; Sundström, V. *Chem. Phys. Lett.* **1993**, *215*, 388.
- (25) Bagchi, B.; Fleming, G. R.; Oxtoby, D. W. *J. Chem. Phys.* **1983**, *78*, 7375.
- (26) Yoshioka, H.; Nakatsu, K. *Chem. Phys. Lett.* **1971**, *11*, 255.
- (27) Bagchi, B. *Chem. Phys. Lett.* **1985**, *115*, 209.
- (28) Bagchi, B. *Chem. Phys. Lett.* **1987**, *139*, 119.
- (29) Poornimadevi, C. S.; Bagchi, B. *Chem. Phys. Lett.* **1988**, *149*, 411.
- (30) Bagchi, B. *Chem. Phys. Lett.* **1987**, *138*, 315.
- (31) Bagchi, B. *Chem. Phys. Lett.* **1987**, *135*, 553.
- (32) Bagchi, B. *Chem. Phys. Lett.* **1987**, *135*, 558.
- (33) Agmon, N.; Hopfield, J. J. *J. Chem. Phys.* **1983**, *78*, 6947.
- (34) Saltiel, J.; D'Agostino, J. T. *J. Am. Chem. Soc.* **1972**, *94*, 6445.
- (35) Saltiel, J.; Sun, Y.-P. *J. Phys. Chem.* **1989**, *93*, 6246.
- (36) Saltiel, J.; Waller, A. S.; Sears, D. F. *J. Am. Chem. Soc.* **1993**, *115*, 2453.
- (37) Todd, D. C.; Fleming, G. R. *J. Chem. Phys.* **1993**, *98*, 269.
- (38) Ben-Amotz, D.; Harris, C. B. *J. Chem. Phys.* **1987**, *86*, 4856.
- (39) Waldeck, D. H.; Fleming, G. R. *J. Phys. Chem.* **1981**, *85*, 2614.
- (40) Keery, K. M.; Fleming, G. R. *Chem. Phys. Lett.* **1982**, *93*, 323.
- (41) Rothenberger, G.; Negus, D. K.; Hochstrasser, R. M. *J. Chem. Phys.* **1983**, *79*, 5360.
- (42) Lee, M.; Bain, A. J.; McCarthy, P. J.; Han, C. H.; Haseltine, J. N.; Smith, A. B.; Hochstrasser, R. M. *J. Chem. Phys.* **1986**, *85*, 4341.
- (43) Hicks, J.; Vandersall, M.; Barbarogic, Z.; Eienthal, K. B. *Chem. Phys. Lett.* **1985**, *116*, 18.
- (44) Stanton, S. G.; Pecora, R.; Hudson, B. S. *J. Chem. Phys.* **1983**, *78*, 3365.
- (45) Goulay, A. M. *J. Chem. Phys.* **1983**, *79*, 1145.
- (46) Ben-Amotz, D.; Scott, T. W. *J. Chem. Phys.* **1987**, *87*, 3739.
- (47) Zhu, S.-B.; Lee, J.; Robinson, G. W. *J. Chem. Phys.* **1988**, *88*, 7088.
- (48) Bagchi, B.; Oxtoby, D. W. *J. Chem. Phys.* **1983**, *78*, 2735.
- (49) Lee, J.; Zhu, S.-B.; Robinson, G. W. *J. Phys. Chem.* **1987**, *91*, 4273.
- (50) Hynes, J. T. *J. Stat. Phys.* **1986**, *42*, 149.
- (51) Grote, R. F.; Hynes, J. T. *J. Chem. Phys.* **1980**, *73*, 2715.
- (52) Fleming, G. R.; Hänggi, P. *Activated Barrier Crossing: Applications in Physics, Chemistry and Biology*. World Scientific Publishing Co.: 1993.
- (53) Bagchi, B.; Oxtoby, D. W. *J. Chem. Phys.* **1983**, *78*, 2735.
- (54) Fleming, G. R.; Knight, A. E. W.; Morris, J. M.; Robbins, R. J.; Robinson, G. W. *Chem. Phys. Lett.* **1977**, *49*, 1.
- (55) Myers, A. B.; Pereira, M. A.; Holt, P. L.; Hochstrasser, R. M. *J. Chem. Phys.* **1987**, *86*, 5146.
- (56) Laitinen, E.; Ruuskanen-Järvinen, P.; Rempel, U.; Helenius, V.; Korppi-Tommola, J. E. I. *Chem. Phys. Lett.* **1994**, *218*, 73.